Peer-reviewed version available at *Inorganics* **2018**, *6*, 79; doi:10.3390/inorganics6030079

Type of the Paper (Article)

On the rehydration of organic layered double hydroxides to form graphene-LDH nanocomposites

Eleonora Conterosito[1], Luca Palin[1,2], Diego Antonioli[1], Maria Pia Riccardi[3], Enrico Boccaleri[1], Maurizio Aceto[1], Marco Milanesio[1,*] and Valentina Gianotti[1,*]

[1] Dipartimento di Scienze e Innovazione Tecnologica, Università del Piemonte Orientale ''A. Avogadro'' (Italy), Via Michel 11, I-15121 Alessandria, Italy.
[2] Nova Res s.r.l., Via Dolores Bello 3, 28100 Novara, Italy. Web: http://www.novares.org
[3] Department of Earth and Environmental Sciences, University of Pavia, Via Ferrata 7, Pavia, Italy
Arvedi Laboratory, CISRIC - University of Pavia, Via Ferrata 7, Pavia, Italy
* Correspondence: valentina.gianotti@uniupo.it; Tel.: +39-0131-360271 for the materials preparation and marco.milanesio@uniupo.it; Tel.: +39-0131-360226 for the materials characterization

Abstract: A graphene-containing LDH was prepared by re-hydration of the oxides produced by the calcination of an organic LDH. While the memory effect is a widely recognized effect on oxides produced by inorganic LDHs, it is unprecedented from the calcination/re-hydration of organic ones. Different temperatures (400, 600 and 1100°C) were tested, on the basis of thermogravimetric data. Water instead of a carbonate solution was used for the re-hydration, with CO_2 available from water itself and/or air to induce a slower process with an easier and better intercalation of the carbonaceous species within the layers. The samples were characterized by X-ray Powder Diffraction (XRPD), IR and Raman spectroscopy and scanning electron microscopy (SEM). XRPD indicate the presence of carbonate LDH mixed with a layered phase with a larger d-spacing. IR confirmed that the prevailing anion is carbonate, coming from the water used for the re-hydration and/or air. Raman data indicated the presence of low-ordered graphenic species moieties and SEM the absence of separated graphene of graphitic sheets, suggesting an intimate mixing of the carbonaceous phase with reconstructed LDH. Organic LDHs gave better memory effect after calcination at 400°C. Conversely, the graphenic species are observed after rehydration of the sample calcined at 600°C with a reduced memory effect, demonstrating the interference of the carbonaceous phase with LDH reconstruction and the bonding with LDH layers to form a graphene-LDH nanocomposite.

Keywords: Layered Double LDHs; Graphene; Mixed Oxides; Re-Hydration; Memory Effect. X-ray Diffraction, Raman Spectroscopy, Scanning Electron Microscopy,

1. Introduction

Layered double hydroxides (LDH) are materials that have attracted a lot of interest in the last years [1–3] thanks to the possibility to act as an host for different inorganic or organic anions that can be intercalated between the mixed metals (e.g. Zn/Al or Mg/Al) hydroxide layers to counterbalance the positive charge of the layer. The applications of layered double hydroxides span from catalysts [4–7] to host for drugs or cosmetics, [8–13] to polymers additives to improve thermal stability and flame resistance [14–17] to adsorbents for decontamination [18–21]. The exchange of the anion and the intercalation of organic anions can be achieved in different ways, which are covered extensively in the literature [3]. One of the methods used in particular for the intercalation of large organic anions is reconstruction upon hydration by exposure to air or to a solution containing the organic anion after the calcination of the inorganic LDH, exploiting the so called "memory effect" [22] of

LDHs. The memory effect is an intriguing property of LDH and it consist in the ability of recovering the LDH structure after its collapse induced by thermal treatment [23–25]. The maximum temperature allowing the reconstruction of the structure depends on the LDH type but it is usually below 500°C [26]. While there are many papers regarding the thermal characterization of the phase changes induced on inorganic LDHs by thermal treatment [27–30] and their reconstruction [24–26,31] the number of studies on this aspect for hybrid LDHs is rather limited [32–34]. The rehydration can be carried out by a carbonate solution [35] or deionized water with carbonate coming from CO_2 in the water itself/and or air [36] [37] [38].The re-hydration is of course facilitated and faster when carbonate is given in stoichiometric ratio or excess amount in the solution used for the reconstruction.

In this work we tried to investigate the less known part of the "memory effect", e.g. the hydration of oxides obtained by calcination of organic LDHs, with the goal of obtaining layered phases, mixed to carbonaceous graphene-like layers. Thermal treatments of both inorganic and organic LDHs were carried out by a TGA experiment to have better control and to be able to track the weight loss. X-ray Powder diffraction was used to assess the degree of reconstruction and IR spectroscopy to identify the anionic species. Finally, a Raman spectroscopy combined to scanning electron microscopy study was performed on the carbon-containing LDHs to confirm the presence of graphene-like low-ordered carbonaceous phases, mixed and/or intercalated within LDHs.

2. Results

2.1. Sample preparation and TGA and XRPD analysis

Two samples were chosen for this study. The first sample is an hybrid Zn/Al LDH intercalated with the NSAID drug Flurbiprofen (Flur) and obtained by Liquid assisted grinding (LAG) method [11,39,40] and hereafter called LDH_Flur. The second sample is the Zn/Al nitrate intercalated LDH used to prepare the hybrid sample, hereafter called LDH_NO_3, as reference material with known "memory effect" properties. TGA was exploited to both identify the best temperature treatments and prepare the calcined samples. In this way, it was possible to follow the calcination and weight loss of the samples treated at the various temperatures (Figure 1). Three temperature were chosen: i) 400°C when a first degradation occurred with a weight loss much smaller with respect to the organic content; ii) 600°C where the degradation of the organic is complete and only a residual carbonaceous phase should be present; iii) 1100°C where the degradation and elimination of organic moieties are complete.

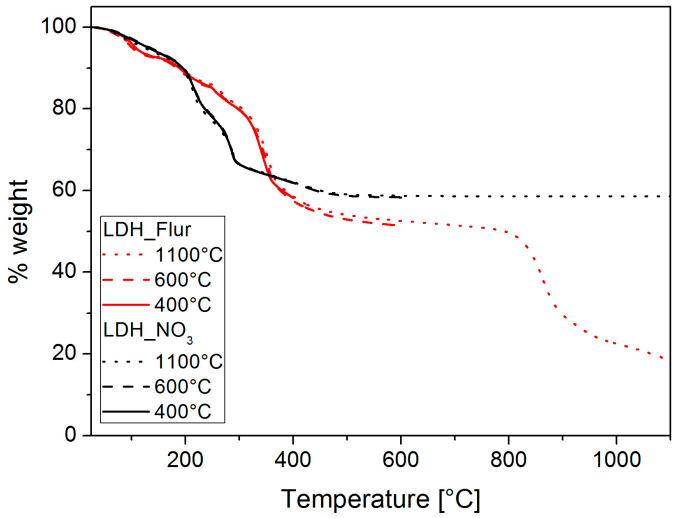

Figure 1: TGA carried out to prepare the samples used for the characterization

The two samples used as starting materials and the three thermal treatments resulted in six final samples summarized in Table 1. Figure 2 reports the XRPD patterns of the starting materials and of flurbiprofen alone as a reference, evidencing a high degree of crystallinity.

Table 1: Sample prepared by thermal treatment in the TGA furnace.

	Temp. treatment (°C)		
Starting Sample	400	600	1100
LDH_NO3	LDH_NO3@400	LDH_NO3@600	LDH_NO3@1100
LDH_Flur	LDH_Flur@400	LDH_Flur@600	LDH_Flur@1100

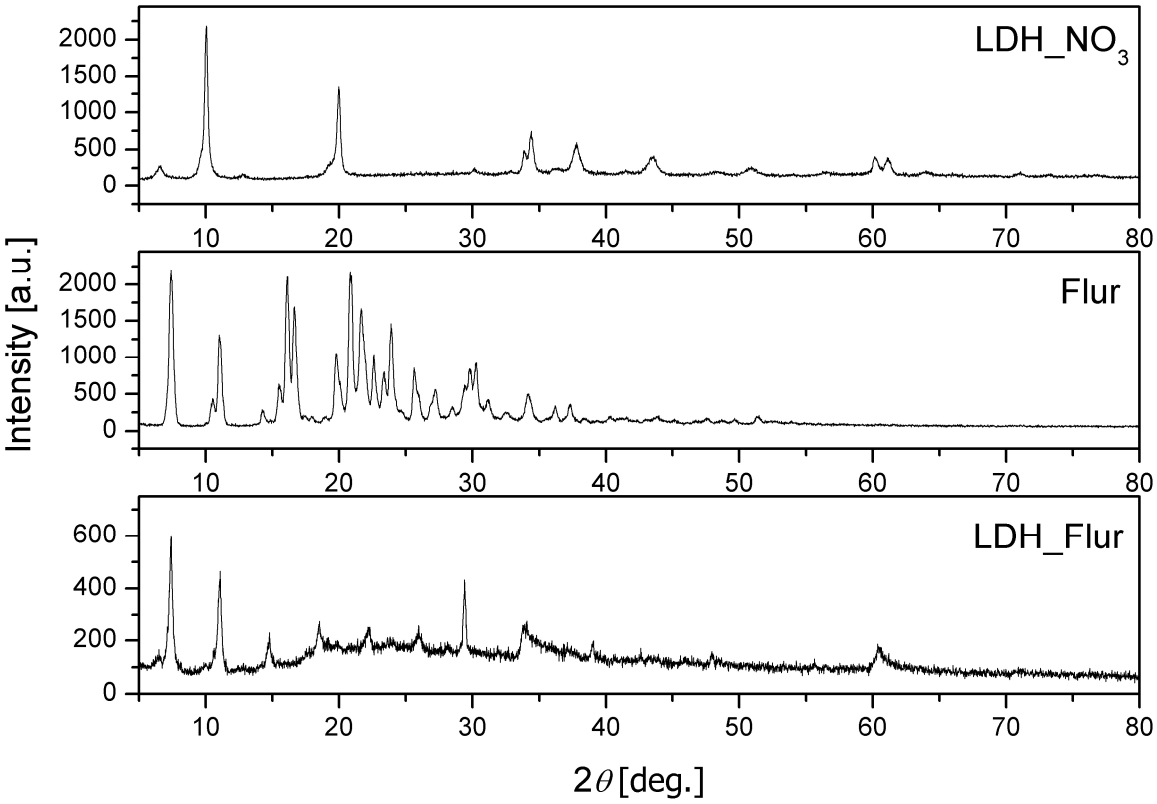

Figure 2: X-ray Powder diffraction of the starting samples.

2.2 Optimization of the re-hydration protocol

The re-hydration was carried out on calcined samples using deionized water instead of a carbonate solution. In this case, carbonate is formed by adsorption of CO_2 from the deionized water and/or the air and fixation. This choice, alternative to using a carbonate solution was done to induce a slower reconstruction process with an easier and better intercalation of the carbonaceous species within the layers. At first, XRPD was carried on the rehydrated samples to assess the degree of reconstruction, calculated as ratio between the LDH and ZnO peaks. In this way, the various protocols used for the re-hydration were tested and optimized. Two approaches were used, also to overcome the problem of the low wettability of the samples, being rather hydrophobic. A first method was a LAG-like approach that consisted in mixing and gently grinding the sample and then adding few drops of distilled water. In a series of preliminary measurements, the re-hydration was repeated at intervals of hours and days, thus alternating hydration and ageing to develop and test the protocol. In a second approach, the hydration was carried out in a sealed vial, to prevent evaporation.

104 *2.2.1 Short-time hydration*

105 To assess the duration of the re-hydration process an *in situ* XRPD experiment was attempted
106 collecting one pattern, limited to the 9-14° 2θ region, every one minute for one hour. These
107 preliminary experiments demonstrated very limited degree of reconstruction in the LDH_NO3@600
108 because the reconstruction is a slow process requiring days and not minutes or hours (see Figure SI-2
109 and Figure 3). Moreover, when measuring in the open sample holder, evaporation is faster than
110 re-hydration, therefore a way of minimizing evaporation resulted mandatory. Therefore, in a second
111 series of experiments the samples were mixed and hydrated in a mortar, covered with a parafilm,
112 then measured after 1 and 24 hours.

113 As a first indication the reconstruction was unsuccessful, independently on the method, on the
114 inorganic sample treated and 1100°C and the residual mass after calcination at 1100°C for the
115 organic samples was a very small difficult to manage amount, the organic samples at the highest
116 temperatures were not characterized.

117

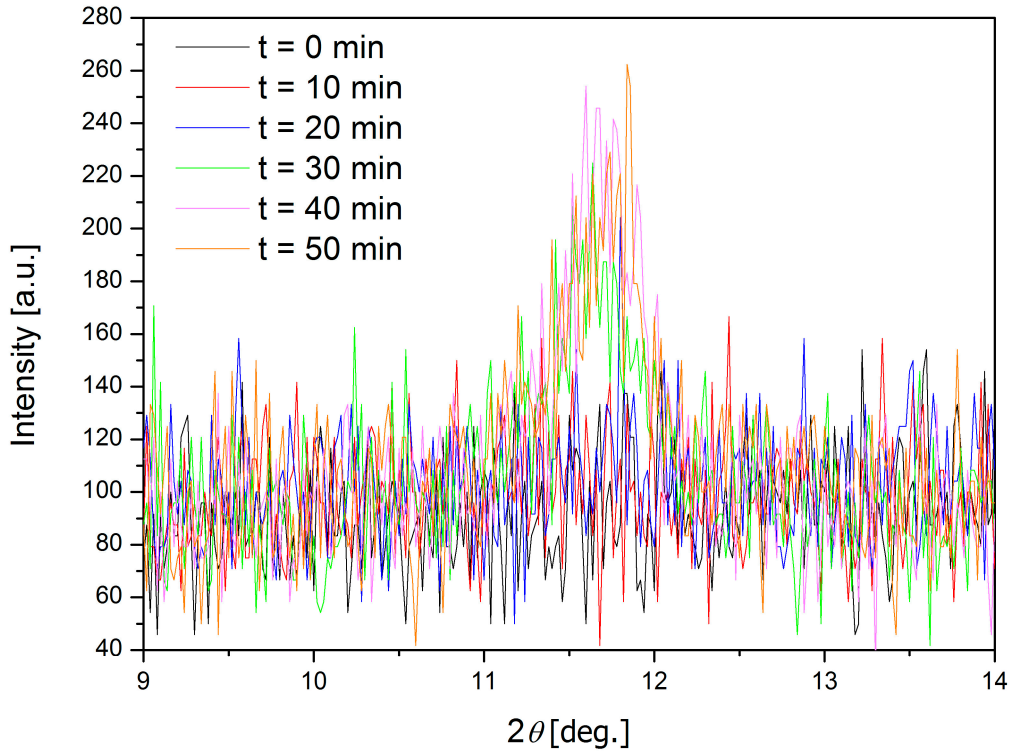

118

119 Figure 3: Selected patterns (one every 10 minutes) from the in situ XRPD experiment on
120 LDH_NO3@600 sample

121

122 In the XRPD pattern of the Zn/Al_LDH_NO_3 sample calcined at 600°C (Fig 4A) the broad band
123 centered at about 23° demonstrate the presence of an amorphous $Al(OH)_3$ phase, while the sharp
124 peaks correspond to crystalline ZnO (ICDD 75-0576). The reconstruction, performed as described in
125 the experimental section was monitored by XRPD within 1 and 72 hours.

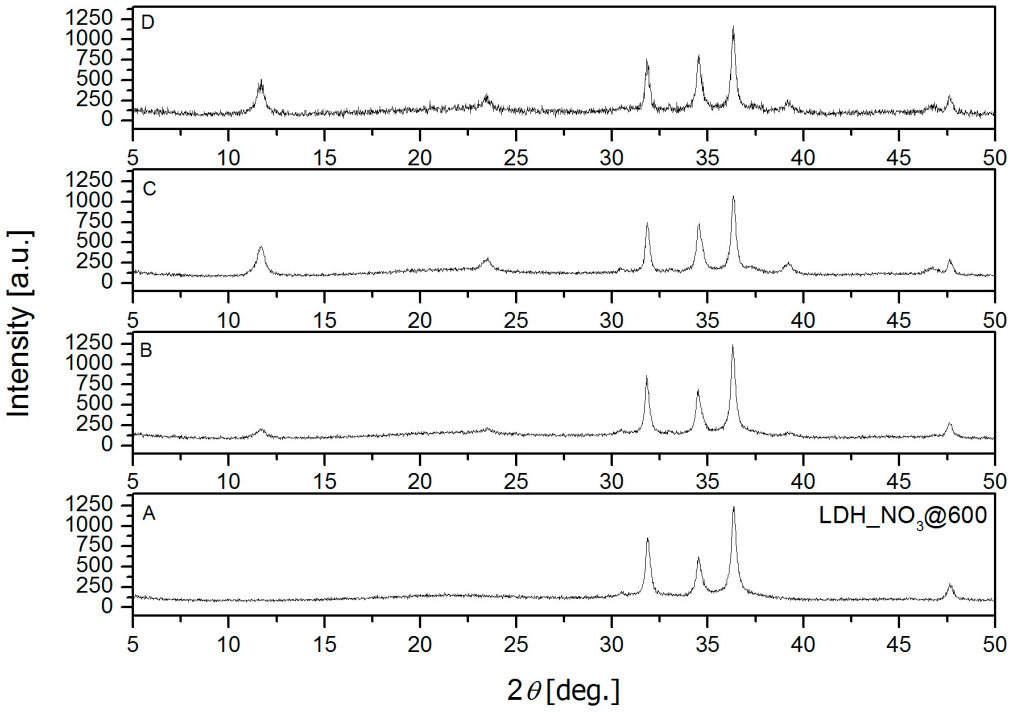

Figure 4: XRPD pattern of the Zn/Al LDH _NO_3 calcined at 600°C (A); after 1 hour rehydration (B), after 24 hours (C), and after 72 hours (D).

It can be noticed that the layered peaks of the LDH structure have appeared at 11.70° and 23.48° but the peaks of ZnO are still present, indicating that the complete reconstruction or the LDH structure is not achieved after 24 hours of rehydration (figure 4C). This is in agreement with Rocha et al. [26], stating that if the calcination temperature exceeds 550°C more time is necessary to achieve full reconstruction. However, in this case even after 72 hours the reconstruction is not complete as demonstrated by the presence of the mixed oxide peaks also in the XRPD pattern collected after 72 hours (figure 4D).

In the XRPD pattern of the Zn/Al_LDH_Flur calcined at 600°C (Fig 4A) there is a large diffraction band between 12* and 29° 2θ attributed to $Al(OH)_3$ and the ZnO peaks as in the Zn/Al_LDH_NO_3 sample..

The in situ rehydration experiment of LDH_Flur@600 was performed as described in the experimental section, using the same protocol of the inorganic LDH. No appearance of the LDH peaks was observed at any time, indicating that reconstruction did not occur in this case, as can be seen in Figure 5, where the XRPD patterns collected after 72 hours are shown and in Figure SI-2 showing the patterns collected during the *in situ* experiment.

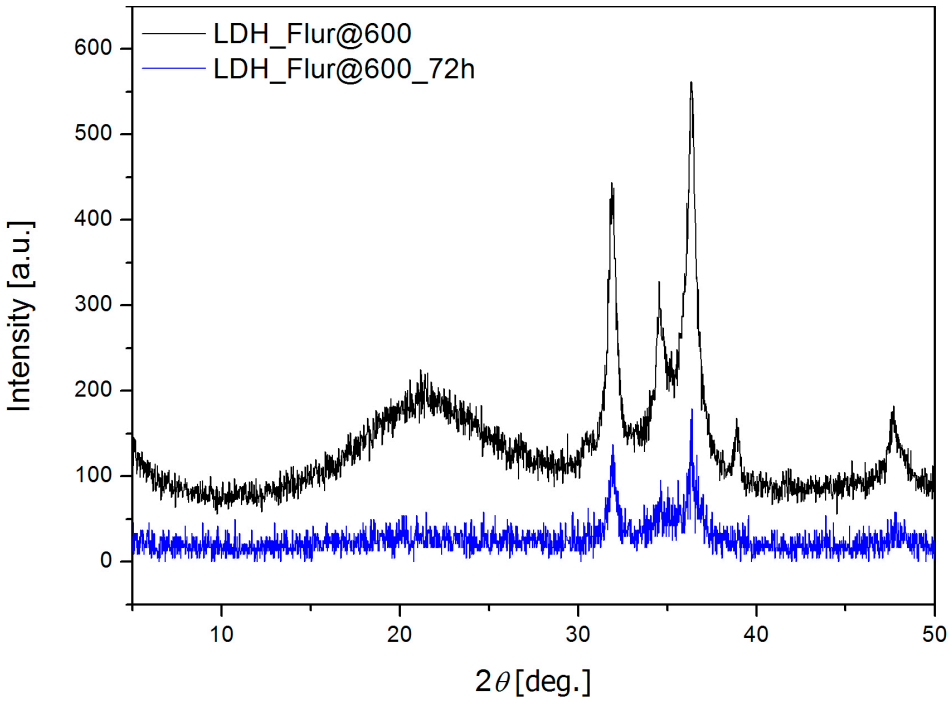

Figure 5: XRPD pattern of the Zn/Al LDH_Flur calcined at 600°C (blue) and after 72 hours (black).

The sample of Zn/Al_LDH_Flur calcined at 1100°C was also analyzed by XRPD. The pattern, shown in figure SI-3 shows the presence of the broad band of $Al(OH)_3$ and the ZnO peaks. Moreover, a spinel $ZnAl_2O_4$ phase is present, matching the mineral Gahnite. The presence of this phase, typical of LDHs calcined above 1000°C, is known to inhibit the reconstruction [26], and in fact no change of the XRPD pattern occurs during the rehydration experiment.

Therefore, the samples treated at 1100°C were abandoned, concentrating the interest on 400°C and 600°C ones. Moreover, the hydration protocol was changed to allow a longer hydration, while preventing evaporation.

2.2.2 Long-time hydration in a vial

A sealed vial was chosen and the time was increased to 14 days then hydration is repeated and prolonged to 28 days, as detailed in the experimental section The samples obtained by the longer re-hydration in a sealed vial are listed in Table 2. In this case a good degree of reconstruction was obtained (Figure 6). Repeating the hydration helped obtaining an high reconstruction yield and incresed crystallinity (see CS_L values obtained by Rietveld refinement of XRPD data in table 3), expecially in the case of the organic containing LDH.

Table 2: Summary of samples and treatments

	Treatment temp (°C)	
Starting sample	14 days hydration	28 days hydration
LDH_NO_3@400	LDH_NO_3@400_14d	LDH_NO_3@400_28d
LDH_Flur@400	LDH_Flur@400_14d	LDH_Flur@400_28d
LDH_NO_3@600	LDH_NO_3@600_14d	LDH_NO_3@600_28d
LDH_Flur@600	LDH_Flur@600_14d	LDH_Flur@600_28d

The XRPD pattern obtained after re-hydration of the inorganic samples (Figure 6 top) indicated that the reconstruction is already good after 14 days, and only a limited increase of the LDH peaks is observed after the second rehydration to arrive to 28 days of ageing. The ZnO oxide peaks are still present evidencing a fraction recalcitrant to hydration also with the long time protocol. In the

organic LDH (Figure 6 top) the second re-hydration gave an important increase of the LDH peaks, especially if the calcination was carried out at 600°C. Moreover, a third phase is observed with peaks corresponding to a layered phase but at larger d-spacing with respect to carbonate LDH.

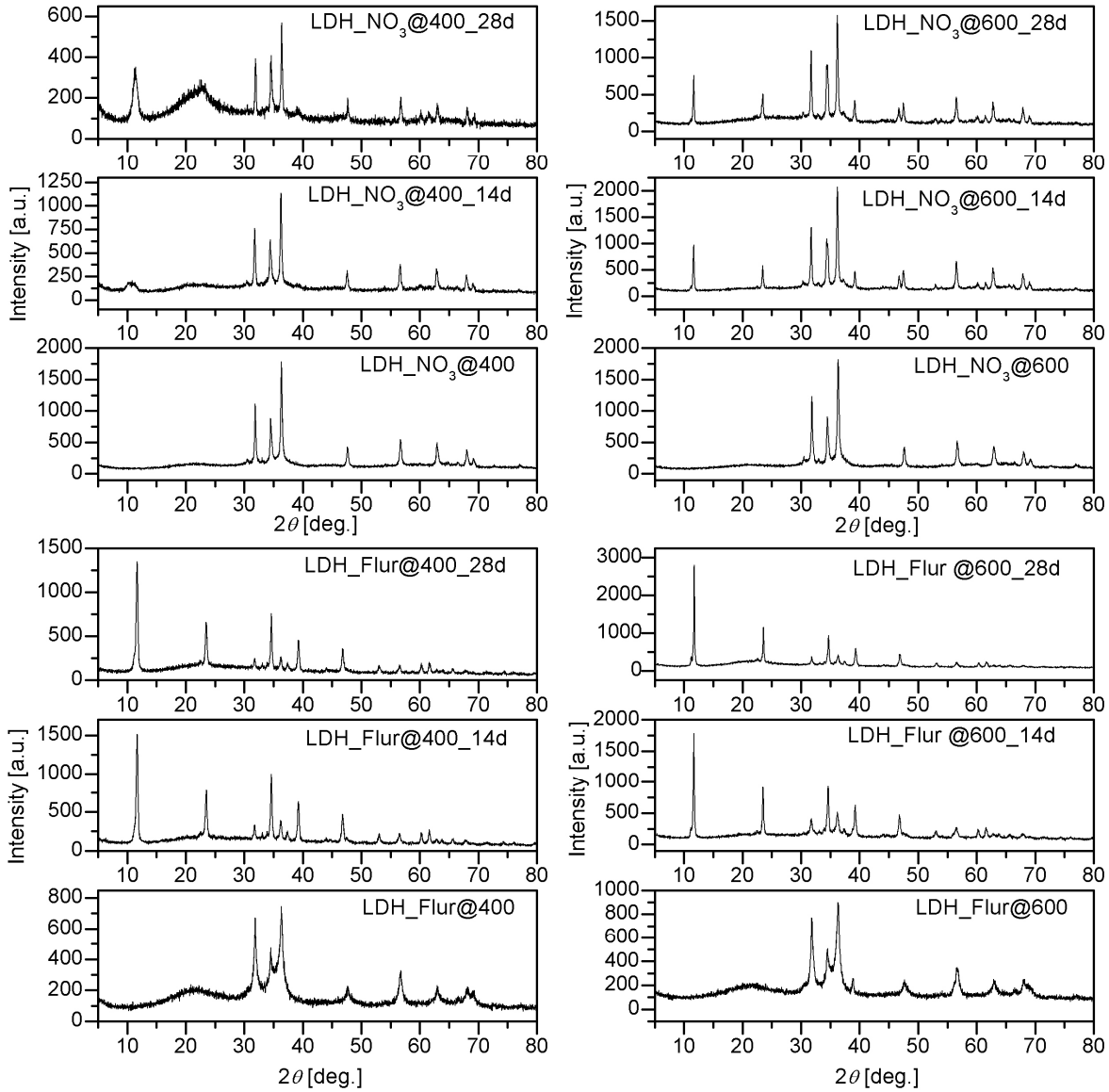

Figure 6: XRPD data before and after 14 and 28 days of ageing for the samples calcined at 400 and 600°C.

To quantify the degree of re-hydration and to investigate the third phase present after rehydration of the organic samples, a Rietveld refinement was carried out (see Figure SI 5-12 and Table 3). To further investigate the nature of the samples a spectroscopic and microscopic investigation is carried out.

Table 3: Results of the Rietveld fit on the samples. The % of the phases and c parameter of the LDH phases are reported.

	% LDH_1	% ZnO	c LDH_1 [Å]	CS_L LDH_1[1]
LDH_NO_3@400_14d	19.04	66.75	23.4(1)	5
LDH_NO_3@400_28d	59.72	40.28	23.6(7)	8
LDH_NO_3@600_14d	26.23	73.77	22.69(4)	77
LDH_NO_3@600_28d	31.36	68.64	22.69(4)	78
LDH_Flur@400_14d	78.75	21.25	22.67(6)	42
LDH_Flur@400_28d	85.33	14.67	22.67(6)	42
LDH_Flur@600_14d	65.30	34.70	22.68(8)	66
LDH_Flur@600_28d	72.90	27.10	22.67(6)	80

[1] Cristallite size parameter (CS_L) of the main LDH phase. Larger values correspond to higher crystallinity.

The Rietveld analyses confirm that the hydration of inorganic LDH_NO_3 sample gave more crystalline LDH if it was calcined at 600°C with respect to 400°C, even if the amount is larger at the lower temperature. Conversely, the hydration of the calcined flurbiprofen-containing sample gave in both cases crystalline LDHs after rehydration, and the sample prepared at 400°C a larger amount (79 vs. 72%) of layered phases. Since the samples after 28 days of reconstruction gave a larger degree of reconstruction, the spectroscopic and morphological characterization was carried out only on these samples. It is moreover noticeable by looking at the XRPD patterns of wet samples (Figure SI-13) how the formation of a larger amount of amorphous phase is correlated to a higher degree of reconstruction when the sample is dried.

2.3. Spectroscopic characterization

A reflectance micro-IR measurement (Figure 7) was carried out to assess the nature of the sample and in particular of the anion after the reconstruction. The optical inspection indicated the presence of black aggregated in the samples prepared form organic LDHs, while it was white for the inorganic ones. In both cases, an evident band at ~1350 cm^{-1} was observed indicating the presence of carbonate. This confirm that the re-hydration occurred intercalating carbon dioxide from both water and air as interlayer anion, thus confirming the great capability of CO_2 absorption of the prepared oxides.

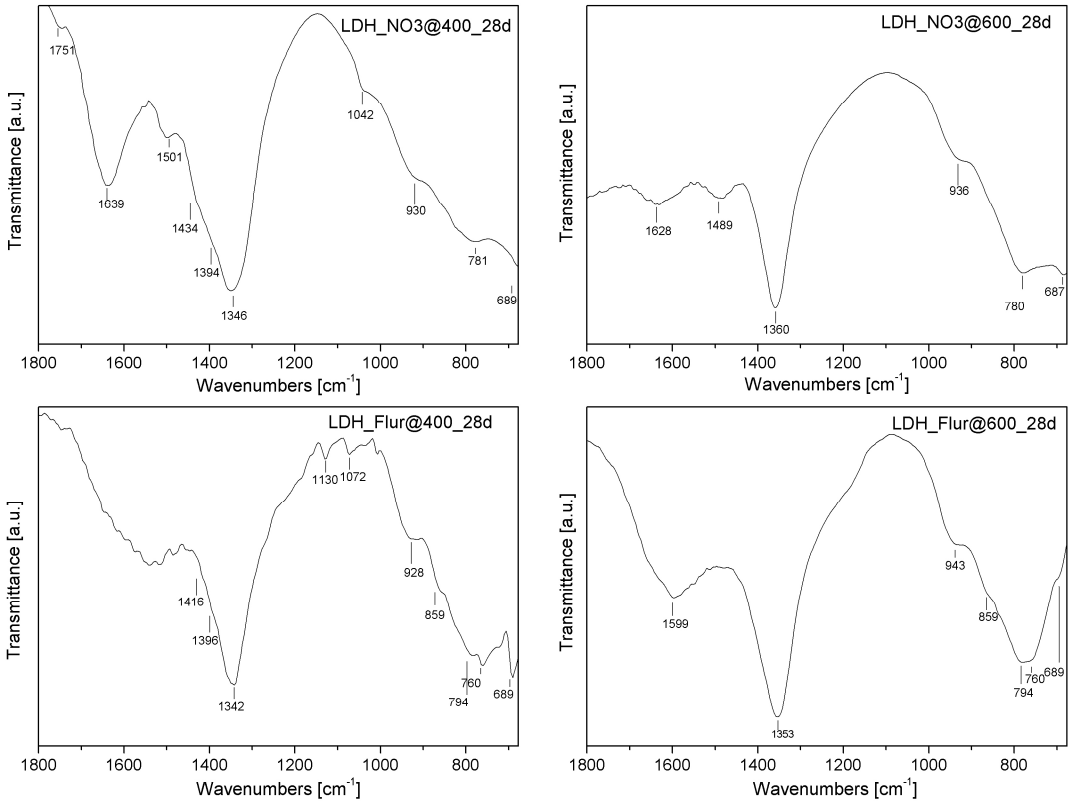

Figure 7: IR reflectance data on the samples after the samples after 28 days of reconstruction.

Raman spectroscopy (Figures 8 and 9) can be employed to further investigate the conversion of species in the rehydration and the fate and conversion of the organic intercalated molecules into carbonaceous species.

Considering the Raman spectra of thermally treated nitrate LDH (Figure 8A), before hydration the sample treated at 400°C highlights the presence of residual nitrate ions (featuring the peak at 1050 cm^{-1}) [28] and a signal around 440 cm^{-1} that, according to literature, can be related to Zn-O/Zn-OH stretching modes [41]. Comparing the calcined samples at 400 and 600°C, the main evidence is the loss of the signal due to nitrate ions, that appear to be completely removed after the treatment at higher temperatures. This is highlighted in the comparison of the spectra reported in figure 8A.

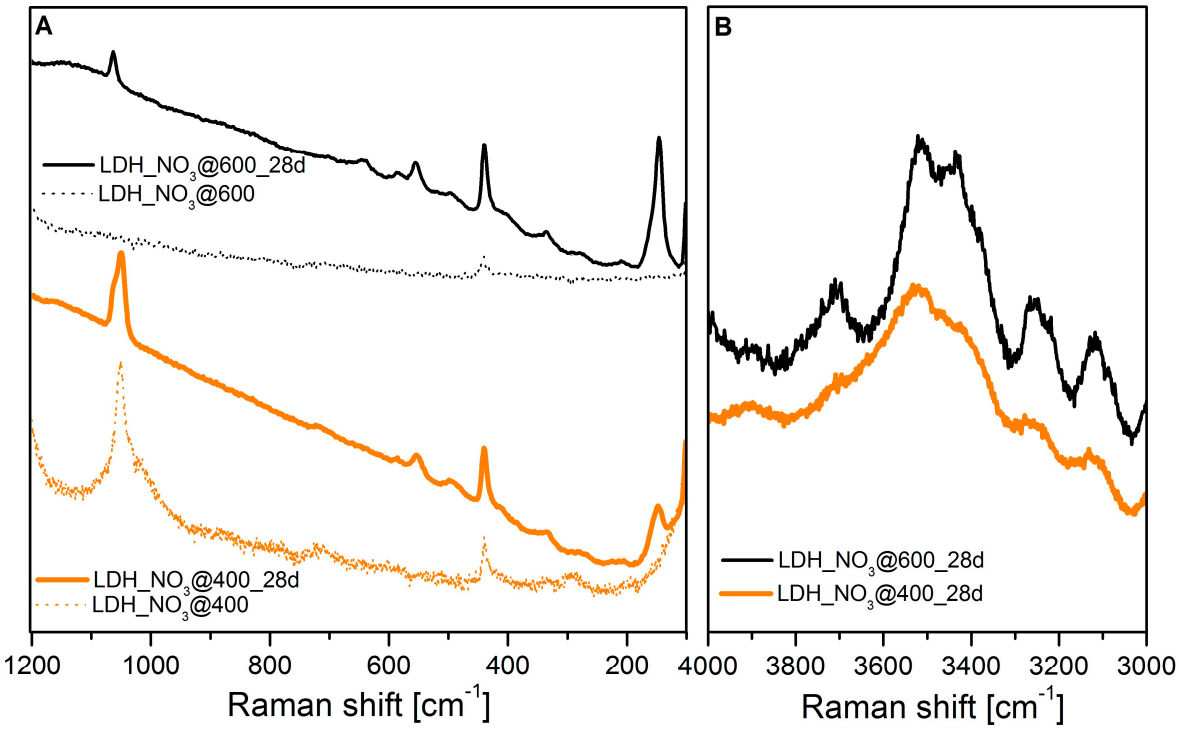

Figure 8: Raman data of LDH_NO3 after calcination at 400°C (orange) and 600°C (black) in the 1200 – 100 cm^{-1} range (A) and in the 4000 – 3000 cm^{-1} range (B) before rehydration (dotted lines) and after two hydrations and a total of 28 days of ageing (solid lines). Raman spectra are collected on the same on the same instrument with red laser (633 mn) for samples before hydration and green laser (532 nm) for doubly hydrated samples.

Upon the recovery of the structure due to hydration, two main contributions appear in the spectra of the samples treated at 400 and 600°C respectively. The peaks at low frequency (around 150, 440, 495 and 550 and minor signals between 250 and 350 cm^{-1} in Figure 8A) [42] of the sample treated at 400°C can be evidences of the recovery of hydroxylic layered structure. The sample at 400°C, highlights the shouldering of the nitrate peak by a component at higher frequency due to the formation of carbonate ions, with a typical Raman peak at 1060 cm^{-1}. The sample treated at 600°C after recovery differs from the sample treated at 400°C for the increase of the intensity of the layered structure vibrational features, but in particular for the signals related to the interlayer ions. In this case, the most evident aspect is the formation of CO_3^{2-} anions as unique species, highlighted by the presence of the related peak at 1060 cm^{-1}. Comparing the spectra, Raman profiles confirm that the higher the temperature of treatment, the higher the extent of decomposition of nitrate ions and of the conversion of layered hydroxides to $ZnO/Al(OH)_3$ species, and the greater the effectiveness of the structural recovery. A further evidence between these two samples can be noted in the hydroxyl stretching region shown in the (Figure 8B), where samples treated at 400 and 600°C reveal the gradual formation of the patterned profile reported in literature, consisting in three bands at around 3355–3360, 3440–3455 and 3535–3580 cm^{-1} [42] .

Conversely, the samples originating from flurbiprofen- intercalated analogues (Figure 9) show only very weak signals coming from the inorganic fraction, close to the 300-500 cm^{-1} region (spectra of nitrate analogues are reported in Figure 8 for comparison). This weakness is due to the overwhelming absorption and fluorescence of the carbonaceous fraction with respect to the inorganic one. In this case, the presence of an organic molecule interleaving the hydroxide structure induces a fully different decomposition/reconstruction pathway. Upon thermal treatment, flurbiprofen is thermally decomposed to carbonaceous fractions (this occurs even at 400°C, where no signals of flurbiprofen features are found in the Raman and IR spectra) and weak broad signals around 1330 and 1590 cm^{-1} can be inferred, as witnesses of the beginning of formation of a

carbonaceous species (Figure 9A and B, green curve) [41]. The extent and diffusion of this carbon-based moieties is highlighted by the 1300-1600 cm^{-1} region of the Raman spectrum of the sample treated at 600°C (Figure 9 A and B, blue curve); in this case, the spectral features in the interest regions reported above are far more evident and are consistent with an ordered layered structure as graphenic sheets. The signals are observed clearly before (Figure 9A) and still present, although weaker, after (Figure 9B) hydration. The presence of such carbonaceous phases is related to a relevantly different behavior of the inorganic Zn/Al hydroxide layers. Raman spectroscopy confirms the presence of graphenic species, even if their location, within the layers of LDHs or as separated entities, could still not be demonstrated.

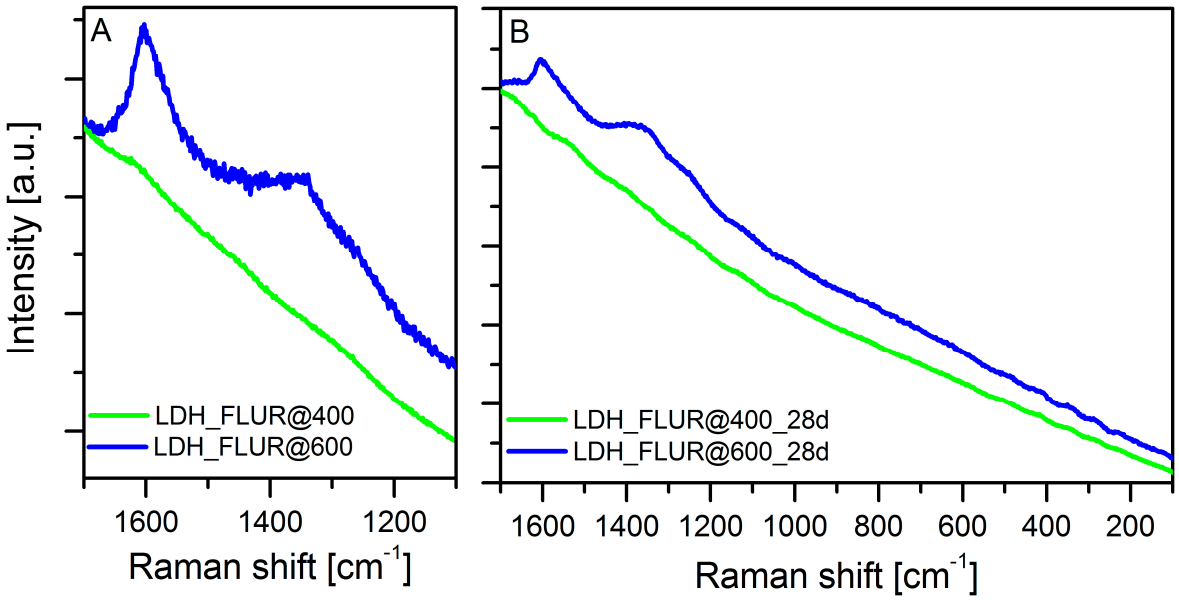

Figure 9: Raman data (green laser excitation) of LDH_FLUR after calcination at 400°C (green) and 600°C (blue) in the 1700 – 1100 cm^{-1} range before rehydration (A).Raman spectra in the range 1700-100 cm^{-1} of the FLUR samples after two hydrations and a total of 28 days of ageing (B).

SEM was used to investigate the morphology of the samples and the location of carbonaceous species. At first, SEM micrograph confirms the larger crystallinity of LDH_NO3@600_28d sample (Figure 10B), where individual lamellar crystallites are clearly observable, with respect to LDH_NO3@400_28d (Figure 10A), where aggregates of smaller crystallites are present, as already suggested by XRPD. The opposite is observed for the samples prepared starting from the organic sample (Figure 10 bottom). This indication confirm that the treatment at 400°C (Figure 10C), with a limited production of graphenic species (as indicated by Raman spectroscopy) allow a better reconstruction, with features similar to those of inorganic samples treated at 600°C. In the sample treated at 600° (Figure 10D) the presence of graphenic species induces a different reconstruction process, with much smaller crystallites. These indications, together with the absence of separated carbonaceous particles or graphitic species in the SEM analysis, strongly suggest that graphenic species are intimately mixed within the reconstructed LDH crystallites.

Peer-reviewed version available at Inorganics 2018, 6, 79; doi:10.3390/inorganics6030079

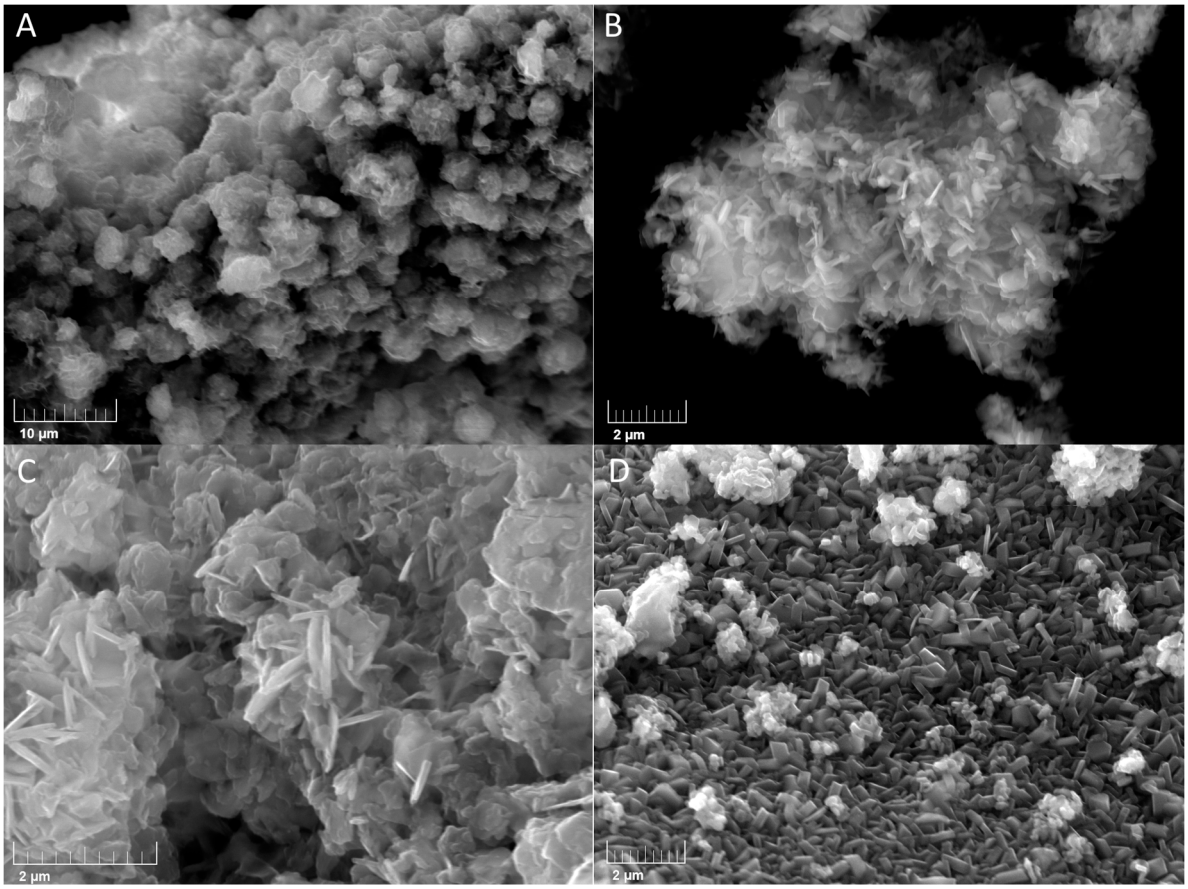

Figure 10: SEM images on the samples after 28 days of reconstruction. A) LDH_NO_3@400_28d (WD 9.30mm, MAG 5.0kx, View field (VF) 57.8µm) B) LDH_NO_3@600_28d (WD 9.34mm, MAG 19.0kx, VF 15.2 µm C) LDH_Flur@400_28d (WD 9.32mm, MAG 35.0kx, VF8.26 µm) D) LDH_Flur@600_28d (WD 8.19mm, MAG 19.0kx, VF 15.2 µm).

3. Discussion

The calcination and re-hydration protocol of organic LDHs was tested and optimized, while an inorganic LDH was used as reference. The process more efficient in giving reconstruction of carbon-containing LDH resulted rather slow, and the highest degree of reconstruction was obtained after a repeated hydration with deionized but not decarbonated water in a sealed vial, with a total of 28 days of ageing. Interestingly, the inorganic samples gave better reconstruction after calcination at 600°C while the organic ones at 400°C. In the samples prepared starting from the flurbiprofen-containing samples, Raman data confirmed the presence of graphenic species in the sample calcined at 600°C. The better reconstruction of the organic sample treated at 400°C is ascribed to the limited production of graphenic species at 400°C, thus allowing a re-hydration process similar to that observed for the inorganic samples. Conversely, the organic sample treated at 600°C, with a much larger amount of graphenic species undergoes a different re-hydration process, with a smaller and more irregular observed crystallites. The absence of XRPD peaks due to graphitic and of graphenic phases in the SEM micrograph suggest that the graphenic species highlighted by Raman after the treatment at 600°C are intimately mixed within LDH reconstructed species, to form a graphene-LDH nanocomposite.

Concerning the mechanism of the reconstruction by the "memory effect" in the two cases (organic and inorganic LDHs), the presence of graphenic species is able to interfere with the LDH reconstruction. A different decomposition mechanism can be inferred. In fact, in nitrate containing materials, the decomposition of nitrate promotes the presence of oxide ions and the reaction between

atomic species on different layers, forming new crystalline phases. When the organic fraction is present, the process of charring either prevents or reduce the formation of oxidic structures at low temperature favoring amorphous hydroxides, but relevantly this phenomenon prevents the interaction of the cationic species distributed on different lamellae of the LDH structure, inducing a markedly different morphology.

4. Materials and Methods

4.1 Sample preparation

Zn/Al LDH_NO_3 of formula [$Zn_{0.66}$ $Al_{0.34}(OH)_2$] [CO_3]$_{0.17}$ 0.5 H_2O prepared by urea method following the procedures described in the literature [43] [13] was used as starting material to prepare the LDH intercalated with Flurbiprofen (sample LDH_Flur), exploiting the LAG method [39,40,44,45].

The calcination of the samples was obtained by thermal treatments imparted by TGA-GC-MS on LDH_Flur and on the LDH_NO_3. The heating starts at 25 °C and, by a heating rate of 10°/min, reaches 400 or 600 or 1100°C to obtain the samples LDH_Flur@400, LDH_Flur@600, LDH_Flur@1100 and LDH_NO3@400, LDH_NO_3@600, LDH_NO_3@1100, respectively.

The re-hydration processes were carried out in two modes. The short-time hydration was performed mixing for 3 minutes approximately 20 mg of calcined sample in a mortar with 60 µL of deionized water, then the mortar was kept covered with parafilm for 72 hours. The XRPD characterizations were performed after 75 minutes, 24 hours and after 72 hours. The long-time re-hydration was performed by mixing for 3 minutes 20 g of calcined sample in a mortar with 60 µL of deionized water, and then storing the sample in sealed vials to prevent evaporation. After 14 days the samples were characterized by XRPD and then put in contact again with 60 µL of deionized water and aged in a sealed vial for 14 days to reach a total of 28 days of ageing. These samples were characterized by XRPD, SEM, IR and Raman spectroscopy.

4.2 Instrumental methods

Thermogravimetric analysis were performed using a Mettler-Toledo thermo-balance TGA/SDTA LF1100 at a scanning rate of 10°C/min from room temperature to 1100 °C under N2.

Static X-ray measurements were performed on a ThermoARL powder diffractometer XTRA, equipped with a solid state Peltier cooled detector. All powder diffraction patterns were measured in continuous mode using the following conditions: 2θ angular range 5-80°, tube power 45kV and 40mA, step size 0.02° 2θ, Integration time: 1,200 sec, Scan rate: 1,000°/min, In situ measures were performed in the range 9-14° 2θ with a scan rate of 5,000°/min on the sample hydrated in the mortar as discussed in section 4.1

IR spectra were recorded on a Nicolet™ iN™ iN10 Infrared Microscope using the LN-cooled MCT detector to enhance sensitivity. Measurements were performed in reflection mode and then the plots were converted in % Transmittance to compare them with standard transmission IR spectra. Each spectra is the average of 128 scans over an area of 150 x 150 µm.

Raman spectra have been collected three instrumentations with different lasers, to minimize the fluorescence problems on different samples and optimize signal detection. The final measurements were carried out exploiting the green laser excitation.

The first was a FT-Raman RFS-100 Bruker instrument equipped with a 1.5 W Nd:YAG air-cooled laser delivering an excitation wavelength of 1064 nm. The detector was a liquid nitrogen cooled germanium detector, allowing a spectral range 3500 to 50 (stokes) and -100 to -2000 cm^{-1} (anti-stokes).

The second was a Renishaw inVia Reflex (Renishaw PLC, UK) microRaman spectrophotometer equipped with a cooled charge-coupled device camera at excitation wavelength of 514.5 nm with a laser power of 10 mW (spectral resolution and integration time of 3 cm^{-1} and 10 s, respectively).

The third was a high-resolution dispersive Horiba Jobin Yvon (Villeneuve d'Ascq, France) Labram HRVIS model system, with an HR800 spectrometer, a confocal microscope, a 800 mm path monochromator and a CCD cooled detector (-70°C). Nd solid state green laser (wavelength 532 nm, power 250 mW) and 1800 lines/mm grating were used, with a spectral resolution of 2 cm^{-1}. Spectra have been taken placing the samples on the microscope stage and observing with long working distance 10x, 20x, 50x and 100x Olympus objectives. The sampled area was identified and focused using either a video camera or microscope binoculars. Spectra were obtained using laser at full power and checking visually with the camera view the absence of damages in the sampling area. Once optimized, spectra have been collected with variable exposure times (1 to 30 seconds) or high number of acquisitions of short shots (10 acquisitions of 1 seconds then averaged) depending on the absolute counting given by the detector.

Raman spectroscopy and XRPD data were analyzed with OPUS [46] and TOPAS Academic v5.0 [47] software respectively.

Textural and morphological observations (secondary electrons images - SE) were performed by means of a Tescan FE-SEM (Mira 3XMU-series), equipped with an EDAX energy-dispersive spectrometer. The operating conditions were: 20 kV accelerating voltage, around 13 mA beam current, different working distance and magnifications (reported in each photo). Samples for SEM observations were prepared either by C-coating from graphite evaporation.

Acknowledgements

This research is original and had a financial support of the Università del Piemonte Orientale within the RICLOCK project.

Author Contributions:

Conceptualization, Eleonora Conterosito and Marco Milanesio; Data curation, Luca Palin; Formal analysis, Eleonora Conterosito; Investigation, Eleonora Conterosito, Luca Palin, Diego Antonioli, Maria Pia Riccardi, Enrico Boccaleri, Maurizio Aceto and Valentina Gianotti; Methodology, Enrico Boccaleri, Marco Milanesio and Valentina Gianotti; Supervision, Marco Milanesio and Valentina Gianotti; Writing – original draft, Eleonora Conterosito and Marco Milanesio; Writing – review & editing, Valentina Gianotti.

Conflicts of Interest

The authors declare no conflict of interest.

References

1. Del Hoyo, C. Layered double hydroxides and human health: An overview. *Appl. Clay Sci.* **2007**, *36*, 103–121, doi:10.1016/j.clay.2006.06.010.

2. Duan, X.; Evans, D. G. *Layered Double Hydroxides*; Duan, X., Evans, D. G., Eds.; Structure and Bonding; Springer-Verlag: Berlin/Heidelberg, 2006; Vol. 119; ISBN 3-540-28279-3.

3. Conterosito, E.; Gianotti, V.; Palin, L.; Boccaleri, E.; Viterbo, D.; Milanesio, M. Facile preparation methods of hydrotalcite layered materials and their structural characterization by combined techniques. *Inorganica Chim. Acta* **2018**, *470*, 36–50, doi:10.1016/j.ica.2017.08.007.

4. Cantrell, D. G.; Gillie, L. J.; Lee, A. F.; Wilson, K. Structure-reactivity correlations in MgAl

hydrotalcite catalysts for biodiesel synthesis. *Appl. Catal. A Gen.* **2005**, *287*, 183–190, doi:10.1016/j.apcata.2005.03.027.

5. Sisani, M.; Costantino, U.; Vivani, R.; Nocchetti, M.; Costantino, F.; Montanari, F.; Cinotti, E. Hydrotalcite-like materials as precursors of catalysts for the production of hydrogen from methanol. *Slides* 2007, 1–41.

6. Othman, M. R.; Helwani, Z.; Fernando, W. J. N. Synthetic hydrotalcites from different routes and their application as catalysts and gas adsorbents: a review. *Appl. Organomet. Chem.* **2009**, *23*, 335–346, doi:10.1002/aoc.1517.

7. Ordóñez, S.; Díaz, E.; León, M.; Faba, L. Hydrotalcite-derived mixed oxides as catalysts for different C–C bond formation reactions from bioorganic materials. *Catal. Today* **2011**, *167*, 71–76, doi:10.1016/j.cattod.2010.11.056.

8. Perioli, L.; Ambrogi, V.; Rossi, C.; Latterini, L.; Nocchetti, M.; Costantino, U. Use of anionic clays for photoprotection and sunscreen photostability: Hydrotalcites and phenylbenzimidazole sulfonic acid. *J. Phys. Chem. Solids* **2006**, *67*, 1079–1083, doi:10.1016/j.jpcs.2006.01.029.

9. Ambrogi, V.; Fardella, G.; Grandolini, G.; Perioli, L.; Tiralti, M. C. Intercalation compounds of hydrotalcite-like anionic clays with anti-inflammatory agents, II: Uptake of diclofenac for a controlled release formulation. *AAPS PharmSciTech* **2002**, *3*, 1–6, doi:10.1007/BF02830624.

10. Ambrogi, V.; Fardella, G.; Grandolini, G.; Nocchetti, M.; Perioli, L. Effect of hydrotalcite-like compounds on the aqueous solubility of some poorly water-soluble drugs. *J. Pharm. Sci.* **2003**, *92*, 1407–18, doi:10.1002/jps.10411.

11. Perioli, L.; Ambrogi, V.; Nocchetti, M.; Rossi, C.; di Nauta, L. Effects of hydrotalcite-like nanostructured compounds on biopharmaceutical properties and release of BCS class II drugs: The case of flurbiprofen. *Appl. Clay Sci.* **2011**, *51*, 407–413, doi:10.1016/j.clay.2010.12.019.

12. Perioli, L.; Ambrogi, V.; Bertini, B.; Ricci, M.; Nocchetti, M.; Latterini, L.; Rossi, C. Anionic clays for sunscreen agent safe use: photoprotection, photostability and prevention of their skin penetration. *Eur J Pharm Biopharm* **2006**, *62*, 185–93, doi:10.1016/j.ejpb.2005.08.001.

13. Costantino, U.; Ambrogi, V.; Nocchetti, M.; Perioli, L. Hydrotalcite-like compounds: Versatile layered hosts of molecular anions with biological activity. *Microporous Mesoporous Mater.* **2008**, *107*, 149–160, doi:10.1016/j.micromeso.2007.02.005.

14. Yang, X.; Zhang, Q. Effect of hydrotalcite on the thermal stability, mechanical properties, rehology and fame retardance of poly(vinyl chloride). *Polym. Int.* **2004**, *53*, 698–707.

15. Liu, J.; Chen, G.; Yang, J. Preparation and characterization of poly(vinyl chloride)/layered double hydroxide nanocomposites with enhanced thermal stability. *Polymer (Guildf).* **2008**,

436 *49*, 3923–3927, doi:10.1016/j.polymer.2008.07.014.

437 16. van der Ven, L.; van Gemert, M. L. .; Batenburg, L. .; Keern, J. .; Gielgens, L. .; Koster, T. P. .;
438 Fischer, H. . On the action of hydrotalcite-like clay materials as stabilizers in
439 polyvinylchloride. *Appl. Clay Sci.* **2000**, *17*, 25–34, doi:10.1016/S0169-1317(00)00002-8.

440 17. Tong, M.; Chen, H.; Yang, Z.; Wen, R. The Effect of Zn-Al-Hydrotalcites Composited with
441 Calcium Stearate and β-Diketone on the Thermal Stability of PVC. *Int. J. Mol. Sci.* **2011**, *12*,
442 1756–66, doi:10.3390/ijms12031756.

443 18. Mohan, D.; Pittman, C. U. Arsenic removal from water/wastewater using adsorbents--A
444 critical review. *J. Hazard. Mater.* **2007**, *142*, 1–53, doi:10.1016/j.jhazmat.2007.01.006.

445 19. Palmer, S. J.; Frost, R. L.; Nguyen, T. Hydrotalcites and their role in coordination of anions in
446 Bayer liquors: Anion binding in layered double hydroxides. *Coord. Chem. Rev.* **2009**, *253*, 250–
447 267, doi:10.1016/j.ccr.2008.01.012.

448 20. Kuzawa, K.; Jung, Y.-J.; Kiso, Y.; Yamada, T.; Nagai, M.; Lee, T.-G. Phosphate removal and
449 recovery with a synthetic hydrotalcite as an adsorbent. *Chemosphere* **2006**, *62*, 45–52.

450 21. Pavan, P. C.; Crepaldi, E. L.; Valim, J. B. Sorption of Anionic Surfactants on Layered Double
451 Hydroxides. *J. Colloid Interface Sci.* **2000**, *229*, 346–352, doi:10.1006/jcis.2000.7031.

452 22. Cavani, F.; Trifirò, F.; Vaccari, A. Hydrotalcite-type anionic clays: preparation, properties and
453 applications. *Catal. Today* **1991**, *11*, 173–301, doi:10.1002/chin.199212317.

454 23. Sato, T.; Wakabayashi, T.; Shimada, M. Adsorption of Various Anions by Magnesium
455 Aluminum Oxide. **1986**, 89–92.

456 24. Roelofs, J. C. A. A.; van Bokhoven, J. a; van Dillen, a J.; Geus, J. W.; de Jong, K. P. The
457 thermal decomposition of Mg-Al hydrotalcites: effects of interlayer anions and characteristics
458 of the final structure. *Chem. Eur. J.* **2002**, *8*, 5571–9,
459 doi:10.1002/1521-3765(20021216)8:24<5571::AID-CHEM5571>3.0.CO;2-R.

460 25. Erickson, K. L.; Bostrom, T. E.; Frost, R. L. A study of structural memory effects in synthetic
461 hydrotalcites using Environmental SEM. **2004**.

462 26. Rocha, J.; del Arco, M.; Rives, V.; Ulibarri, M. A. Reconstruction of layered double hydroxides
463 from calcined precursors: a powder XRD and 27Al MAS NMR study. *J. Mater. Chem.* **1999**, *3*,
464 2499–2503, doi:10.1039/A903231B.

465 27. Kloprogge, J. T.; Frost, R. L. Infrared emission spectroscopic study of the thermal
466 transformation of Mg-, Ni- and Co-hydrotalcite catalysts. *Appl. Catal. A Gen.* **1999**, *184*, 61–71,
467 doi:10.1016/S0926-860X(99)00084-8.

468 28. Kloprogge, J. T.; Wharton, D.; Hickey, L.; Frost, R. L. Infrared and Raman study of interlayer
469 anions CO32-, NO3-, SO42- and ClO4- in Mg / Al- hydrotalcite. *Am. Mineral.* **2002**, *87*, 623–

629.

29. Kloprogge, J. T.; Kristof, J.; Frost, R. L. Thermogravimetric analysis–mass spectrometry (TGA–MS) of hydrotalcites containing CO32-,NO3-,Cl-;SO42- or ClO4-. In *A Clay Odyssey. Proceedings of the 12th International Clay Conference*; Dominguez, E., Mas, G., Cravero, F., Eds.; Bahai-Blanca, Argentina, 2001; Vol. 507–508.

30. Kloprogge, T. J.; Hickey, L.; Frost, R. L.; Kloprogge, J. T.; Hickey, L.; Frost, R. L. Heating stage Raman and infrared emission spectroscopic study of the dehydroxylation of synthetic Mg-hydrotalcite. *Appl. Clay Sci.* **2001**.

31. Wong, F.; Buchheit, R. G. Utilizing the structural memory effect of layered double hydroxides for sensing water uptake in organic coatings. *Prog. Org. Coatings* **2004**, *51*, 91–102, doi:10.1016/j.porgcoat.2004.07.001.

32. Conterosito, E.; Palin, L.; Antonioli, D.; Viterbo, D.; Mugnaioli, E.; Kolb, U.; Perioli, L.; Milanesio, M.; Gianotti, V. Structural Characterisation of Complex Layered Double Hydroxides and TGA-GC-MS Study on Thermal Response and Carbonate Contamination in Nitrate- and Organic-Exchanged Hydrotalcites. *Chem. A Eur. J.* **2015**, *21*, 14975–14986, doi:10.1002/chem.201500450.

33. Conterosito, E.; Croce, G.; Palin, L.; Pagano, C.; Perioli, L.; Viterbo, D.; Boccaleri, E.; Paul, G.; Milanesio, M. Structural characterization and thermal and chemical stability of bioactive molecule/hydrotalcite (LDH) nanocomposites. *Phys. Chem. Chem. Phys.* **2013**, *15*, 13418–13433, doi:10.1039/c3cp51235e.

34. Sun, Y.; Pan, G.; Gu, Q.; Li, X.; Sun, G.; Ma, S.; Yang, X. Structural transformation and photoluminescence behavior during calcination of the layered europium-doped yttrium hydroxide intercalate with organic-sensitizer. *Mater. Res. Bull.* **2013**, *48*, 4460–4468, doi:10.1016/j.materresbull.2013.07.053.

35. Shiraga, M.; Kawabata, T.; Li, D.; Shishido, T.; Komaguchi, K.; Sano, T.; Takehira, K. Memory effect-enhanced catalytic ozonation of aqueous phenol and oxalic acid over supported Cu catalysts derived from hydrotalcite. *Appl. Clay Sci.* **2006**, *33*, 247–259, doi:10.1016/J.CLAY.2006.05.005.

36. Miyata, S. Anion-exchange properties of hydrotalcite-like compounds. *Clays Clay Miner.* **1983**, *31*, 305–311.

37. Valente, J. S.; Figueras, F.; Gravelle, M.; Kumbhar, P.; Lopez, J.; Besse, J.-P. Basic Properties of the Mixed Oxides Obtained by Thermal Decomposition of Hydrotalcites Containing Different Metallic Compositions. *J. Catal.* **2000**, *189*, 370–381, doi:10.1006/JCAT.1999.2706.

38. Zhu, H.; Tang, P.; Feng, Y.; Wang, L.; Li, D. Intercalation of IR absorber into layered double hydroxides: Preparation, thermal stability and selective IR absorption. *Mater. Res. Bull.* **2012**, *47*, 532–536, doi:10.1016/J.MATERRESBULL.2011.12.056.

506 39. Milanesio, M.; Conterosito, E.; Viterbo, D.; Perioli, L.; Croce, G. New Efficient Intercalation of
507 Bioactive Molecules into Layered Double Hydroxide Materials by Solid-State Exchange: An
508 in Situ XRPD Study. *Cryst. Growth Des.* **2010**, *10*, 4710–4712, doi:10.1021/cg1011023.

509 40. Conterosito, E.; Van Beek, W.; Palin, L.; Croce, G.; Perioli, L.; Viterbo, D.; Gatti, G.; Milanesio,
510 M. Development of a Fast and Clean Intercalation Method for Organic Molecules into
511 Layered Double Hydroxides. *Cryst. Growth Des.* **2013**, *13*, 1162–1169, doi:10.1021/cg301505e.

512 41. Boccaleri, E.; Arrais, A.; Frache, A.; Gianelli, W.; Fino, P.; Camino, G. Comprehensive spectral
513 and instrumental approaches for the easy monitoring of features and purity of different
514 carbon nanostructures for nanocomposite applications. *Mater. Sci. Eng. B* **2006**, *131*, 72–82,
515 doi:10.1016/J.MSEB.2006.03.028.

516 42. Kloprogge, J. T.; Hickey, L.; Frost, R. L. FT-Raman and FT-IR spectroscopic study of synthetic
517 Mg/Zn/Al-hydrotalcites. *J. Raman Spectrosc.* **2004**, *35*, 967–974, doi:10.1002/jrs.1244.

518 43. Costantino, U.; Nocchetti, M.; Vivani, R.; Marmottini, F. New synthetic routes to
519 hydrotalcite-like compounds - Characterisation and properties of the obtained materials. *Eur.*
520 *J. Inorg. Chem.* **1998**, 1439–1446,
521 doi:10.1002/(SICI)1099-0682(199810)1998:10<1439::AID-EJIC1439>3.0.CO;2-1.

522 44. Toson, V.; Conterosito, E.; Palin, L.; Boccaleri, E.; Milanesio, M.; Gianotti, V. Facile
523 Intercalation of Organic Molecules into Hydrotalcites by Liquid-Assisted Grinding: Yield
524 Optimization by a Chemometric Approach. *Cryst. Growth Des.* **2015**, *15*, 5368–5374,
525 doi:10.1021/acs.cgd.5b00968.

526 45. Conterosito, E.; Milanesio, M.; Palin, L.; Gianotti, V. Rationalization of liquid assisted
527 grinding intercalation yields of organic molecules into layered double hydroxides by
528 multivariate analysis. *RSC Adv.* **2016**, *6*, 108431–108439, doi:10.1039/C6RA17769G.

529 46. *OPUS Version 5.5*; Copyright Bruker Optik GmbH;

530 47. Coelho, A. A. *Topas-Academic. General Profile and Structure Analysis Software for Powder*
531 *Diffraction Data, version, 5.*; 2012.